Stress-constrained topology optimization: a topological level-set approach

Krishnan Suresh & Meisam Takalloozadeh

Structural and Multidisciplinary Optimization

ISSN 1615-147X
Volume 48
Number 2

Struct Multidisc Optim (2013)
48:295-309
DOI 10.1007/s00158-013-0899-4

Springer

Struct Multidisc Optim (2013) 48:295–309
DOI 10.1007/s00158-013-0899-4

RESEARCH PAPER

Stress-constrained topology optimization: a topological level-set approach

Krishnan Suresh · Meisam Takalloozadeh

Received: 31 August 2012 / Revised: 21 January 2013 / Accepted: 24 January 2013 / Published online: 9 March 2013

Abstract The objective of this paper is to introduce and demonstrate an algorithm for stress-constrained topology optimization. The algorithm relies on tracking a *level-set* defined via the topological derivative. The primary advantages of the proposed method are: (1) the stresses are well-defined at all points within the evolving topology, (2) the finite-element stiffness matrices are well-conditioned, making the analysis robust and efficient, (3) the level-set is tracked through a simple iterative process, and (4) the stress constraint is precisely satisfied at termination. The proposed algorithm is illustrated through numerical experiments in 2D and 3D.

Keywords Topology optimization · Stress · Level set

1 Introduction

Topology optimization plays an important role in structural design today. It has rapidly evolved from an academic exercise into an exciting discipline with numerous industrial applications.

The most common topology optimization problem is that of compliance-minimization. As an illustrative example, consider the plane-stress problem over the domain D in Fig. 1. A compliance minimization problem, assuming a finite element discretization for the underlying elasticity problem, may be posed as Eschenauer and Olhoff (2001) and Rozvany (2009):

$$\begin{aligned} &\underset{\Omega \subset D}{Min}\ J \\ &|\Omega| \leq v_0 \text{ in } \Omega \\ &\text{subject to} \\ &Ku = f \end{aligned} \tag{1.1}$$

where:

$$\begin{aligned} u &: \text{ Finite element displacement field} \\ K &: \text{ Finite element stiffness matrix} \\ f &: \text{ External force vector} \\ J &: \text{ Compliance} = u^T f \\ v_0 &: \text{ Maximum allowable volume} \\ \Omega &: \text{ Topology to be computed} \\ D &: \text{ Region within which the topology must lie} \end{aligned} \tag{1.2}$$

Thus the objective is to find the (optimal) topology of a given volume fraction with least compliance.

Before the above problem can be solved, optimization parameters must be defined that capture the evolving topology; see Rozvany (2009) and Bendsoe and Sigmund (2003) for a review. In Solid Isotropic Material with Penalization (SIMP), the optimization parameters are the density variables assigned, usually to each finite element. These density variables define the topology as described, for example in Sigmund (2001). On the other hand, in level-set methods (Allaire et al. 2002; Allaire and Jouve 2005; He et al. 2007; Wang et al. 2003), the topology is defined and controlled via an auxiliary function. The reader is referred to Guo et al. (2011) for a thorough mathematical treatment of the level-set based formulation.

K. Suresh (✉)
Mechanical Engineering, University of Wisconsin,
Madison, WI, USA
e-mail: suresh@engr.wisc.edu

M. Takalloozadeh
Civil Engineering, Sharif University of Technology, Tehran, Iran

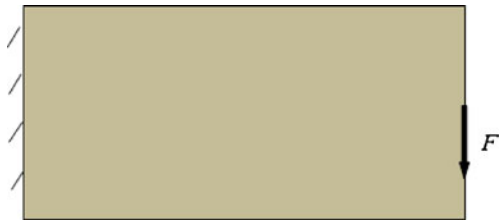

Fig. 1 A structural problem

In *stress-constrained* topology optimization, the underlying problem may be posed as:

$$\begin{aligned} &\underset{\Omega \subset D}{Min} \; |\Omega| \\ &\sigma \leq \sigma_{\max} \text{ in } \Omega \\ &J \leq J_{\max} \\ &\text{subject to} \\ &Ku = f \end{aligned} \tag{1.3}$$

where:

$$\begin{aligned} &\sigma \text{ : von Mises Stress} \\ &\sigma_{\max} \text{ : Max allowable von Mises Stress} \\ &J_{\max} \text{ : Max compliance allowed} \\ &\Omega \text{ : Topology to be computed} \\ &D \text{ : Region within which the topology must lie} \end{aligned} \tag{1.4}$$

The objective here is to find the (optimal) topology of least volume subject to stress and compliance constraint. Note that the compliance constraint is required to avoid the pathological case of zero volume topology that satisfies the stress constraint trivially (Guo et al. 2011). The compliance constraint is critical and handled later in the paper. Such stress constrained problems are harder to solve than compliance problems (Yang and Chen 1996), and arguably more important (Duysinx et al. 2008).

Current methods for solving stress-constrained topology optimization problems are reviewed in Section 3. In this paper, a new topological sensitivity (Sokolowski and Zochowski 1999) based method is proposed. The concept of topological sensitivity is reviewed in Section 3. This is followed by a detailed description of the proposed method in Section 4. In Section 5, numerical results are presented, followed by conclusions and open issues in Section 6.

2 Literature review

Methods for solving stress-constrained topology optimization problems can be classified into two distinct types: SIMP and level-set.

A common challenge to both strategies is resolving the point-wise stress constraints in (1.3), i.e., it is impossible to impose stress constraints at all points within the domain. Therefore, in a finite element implementation, the element-stresses are typically lumped together into a single global quantity via the p-norm (Le et al. 2010), Kreisselmeier–Steinhauser function (Paris et al. 2009), or potentially active constraints (Duysinx and Bendsoe 1998), and global/local penalization (Xia et al. 2012). The equivalence of these two measures, and their justification is discussed, for example, in Qiu and Li (2010). Later in this paper, we shall exploit the p-norm global measure. Alternately, active-set methodologies have also been proposed where a finite number of elements with the highest stress states are chosen to be active during a given iteration (Bruggi and Duysinx 2012; Zhang et al. 2012).

2.1 Solid Isotropic Material with Penalization (SIMP)

The most popular topology optimization strategy today is SIMP where pseudo-densities are assigned to finite-elements, and then optimized to meet the desired objective (Sigmund 2001).

The primary advantage of SIMP is that it is well-developed, but the 'singularity-problem' associated with zero-density elements require careful treatment, for example through epsilon-methods (Guo and Cheng 2004; Le 2010). Secondly, the ill-conditioning of the stiffness matrices, once again due to the low-density elements, can lead to high computational costs for iterative solvers (Wang et al. 2007; Suresh 2013). Additional challenges including stress-ambiguity and accuracy over gray-elements are identified and discussed in Guo et al. (2011).

One of the earliest implementation of SIMP for stress-constrained topology optimization was reported in Yang and Chen (1996), where the authors addressed instability and singularity issues via a weighted combination of compliance and global stress measure. Such concepts continue to play an important role today. In Stump et al. (2007), the authors proposed a framework to design the material distribution of functionally graded structures with a tailored Von Mises stress field. In Paris et al. (2009), the authors studied the weight minimization problems with global or local stress constraints, in which the global stress constraints are defined by the Kreisselmeier–Steinhauser function. In Le (2010), to resolve the stress singularity phenomenon, a SIMP-motivated stress definition was used. In addition, the author used the restriction method with a density filter for length scale control. Finally, a global/regional stress measure combined with an adaptive normalization scheme to control the local stress level. The mixed finite element method (FEM) was proposed for stress-constrained topology optimization, to alleviate the challenges posed by displacement-based FEM (Bruggi and Venini 2008). More recently, the authors of Yalamanchili and Kumar (2012) proposed a *conservative* global stress measure, and the

objective function was constructed using the relationship between mean compliance and von Mises stress,the authors used a SIMP-based mesh-independent framework. In Bruggi and Duysinx (2012) Drucker–Prager failure criterion is considered within the SIMP framework to handle materials with different tension and compression behaviors; a stress-relaxation scheme is proposed to handle the well—known stress singularity.

As an alternate to SIMP, a free material optimization was proposed in Kocvara and Stingl (2012) as a means of addressing the stress singularity in SIMP. Similarly, in Svanberg and Werme (2007), binary design variables were used instead of density variables, and the problem was reduced to that of integer-programming, with guaranteed local minima.

2.2 Level-set

The second strategy for solving stress-constrained topology optimization problems relies on defining the evolving topology via a level-set. Since the domain is well-defined at all times, the singularity problem does not arise, and the stiffness matrices are typically well-conditioned. One of the earliest implementation of level-set based stress-constrained topology optimization appears in Allaire and Jouve (2008) where the authors proposed to minimize a domain integral of stress subject to material volume constraint. A similar approach was explored in James et al. (2012). In particular, to address irregular, i.e., non-rectangular domains, an iso-parametric approach to solving the Hamilton-Jacobi equation was explored by the authors. In the level-set implementation of Xia et al. (2012), a new global stress measure was proposed. In Guo et al. (2011) and Zhang et al. (2012), the authors combine the advantages of level-set with X-FEM for accurate shape and topology optimization. The active-set methodology with augmented Lagrangian is used to alleviate stress-concentrations. Numerous examples are provided to illustrate the effectiveness of their method.

The authors of Amstutz and Novotny (2010) were the first to explore the use of topological derivative in stress-based topology optimization. In particular, they introduced a class of penalty functionals for point-wise constraints on the Von Mises stress field.

3 Technical background

The proposed method rests on the notion of topological sensitivity, reviewed next.

3.1 Topological sensitivity

Topological sensitivity captures the first order impact of inserting a small circular hole within a domain on various quantities of interest. This concept has its roots in the influential paper by Eschenauer et al. (1994), and has later been extended and explored by numerous authors (Sokolowski and Zochowski 1999; Novotny et al. 2005, 2007; Novotny 2006; Céa et al. 2000) including generalization to arbitrary features (Turevsky et al. 2009; Turevsky and Suresh 2007; Gopalakrishnan and Suresh 2008).

Although the focus of this paper is on stress constrained problems, for simplicity, the concept of topological sensitivity is reviewed using compliance minimization.

Consider again the problem illustrated earlier in Fig. 1. Let the initial compliance of the system be J_0.

Suppose we introduce a tiny hole, i.e., modify the topology, as illustrated in Fig. 2, the finite element solution and the compliance will change. Specifically, let an infinitesimal hole of radius r be inserted at point p and let the new compliance be $J(r)$. The topological sensitivity in 2-D is defined as:

$$\mathcal{T}_J(p) \equiv \lim_{r\to 0} \frac{J(r) - J_0}{\pi r^2} \tag{3.1}$$

Using the above definition, the following closed-form expression can be derived for the topological sensitivity (Turevsky and Suresh 2011):

$$\mathcal{T}_J(p) = \frac{4}{1+\nu}\sigma : \varepsilon - \frac{1-3\nu}{1-\nu^2} tr(\sigma) tr(\varepsilon) \tag{3.2}$$

where ν is the Poisson's ratio, σ and ε are the stress and strain tensors respectively at point p (before the hole was inserted). Thus, given the stress and strain field in the original domain (without the hole), one can compute the topological sensitivity over the entire domain; the resulting (scaled) field is illustrated in Fig. 3. Observe that if the topological sensitivity is small (large), then removing material at that point has little (significant) impact on the compliance. In 3-D, the topological sensitivity field for compliance is given by Novotny et al. (2007):

$$\mathcal{T} = -20\mu\sigma : \varepsilon - (3\lambda - 2\mu)\, tr(\sigma) tr(\varepsilon) \tag{3.3}$$

where μ & λ are the Lame parameters.

A simple approach to exploiting topological sensitivity in topology optimization is to 'kill' mesh-elements with low values. However, this leads to instability and checker-board patterns. Alternately, the TS field can be used to introduce

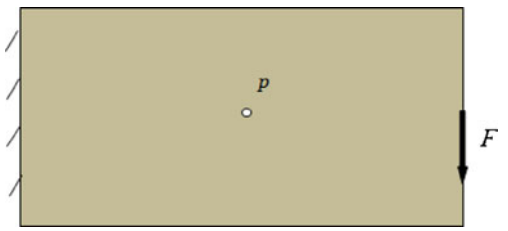

Fig. 2 A topological change

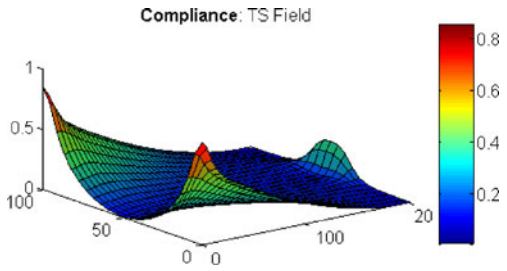

Fig. 3 Topological sensitivity field

holes during the topology optimization process via an auxiliary level-set (Allaire et al. 2004). Finally, the authors in Norato et al. (2007), use the topological sensitivity field with fictitious domain method to enhance the convergence of topology optimization.

Here we consider an alternate and a more powerful approach called "PareTO" where one exploits the topological sensitivity field *directly* as a level-set.

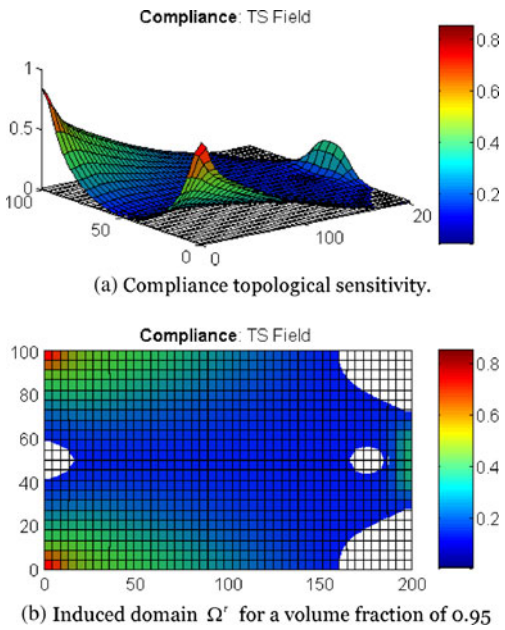

Fig. 4 Topological sensitivity field as a level-set

4 Proposed method

The PareTO method (Suresh 2010) is first discussed below using compliance minimization, and then extended to stress minimization.

4.1 PareTO for compliance minimization

In PareTO, the topological sensitivity field directly serves as a level-set. Associated with the level-set is a cutting-plane. For example, Fig. 4a illustrates again the compliance field T_J and a cutting plane corresponding to an arbitrary cut-off value $\tau = 0.03$. Given the field, and a cutting plane, one can define a domain Ω^τ per:

$$\Omega^\tau = \{\, p \,|\, \mathcal{T}_J(p) > \tau \} \tag{4.1}$$

In other words, the domain Ω^τ is the set of all points where the topological field exceeds τ; the induced domain Ω^τ is illustrated in Fig. 4b. The τ value can be chosen such that, say, 10 % of the volume is removed. Observe how portions of the domain that are least critical for the stiffness of the structure have been eliminated. In other words, a 'pseudo-optimal' domain has been constructed directly from the topological sensitivity field. This is akin to the 'kill method'.

However, the computed domain may not be 'pareto-optimal' (see Suresh 2010), i.e., it is not the stiffest structure for the given volume fraction. One must now repeat the following three steps: (1) solve the finite element problem over Ω^τ (2) re-compute the topological sensitivity, and (3) find a new value of τ for the desired volume fraction. In essence, we carry out a fixed-point iteration (Céa et al. 2000; Norato et al. 2007; Suresh 2013) involving three quantities (see Fig. 5): (1) domain Ω^τ, (2) displacement fields u and v over Ω^τ, and (3) topological sensitivity field over Ω^τ. Typically, convergence is reached in 3 to 4 iterations (Suresh 2013).

Once convergence has been achieved, an additional 10 % volume can be removed by repeating this process. Thus, the overall PareTO algorithm is illustrated in Fig. 6.

Using the above algorithm, the compliance problem posed in (1.1) can be solved, resulting in a series of pareto-optimal topologies as illustrated in Fig. 7. In other words, PareTO, as the name suggests, finds pareto-optimal solutions to the multi-objective problem:

$$\underset{\Omega \subset D}{Min} \{J, |\Omega|\} \tag{4.2}$$

4.2 Stress constrained compliance minimization

One can extend the above method by adding a stress constraint directly to (4.2), resulting in:

$$\begin{aligned} &\underset{\Omega \subset D}{Min}\, \{J, |\Omega|\} \\ &\sigma \leq \sigma_{\max} \text{ in } \Omega \end{aligned} \tag{4.3}$$

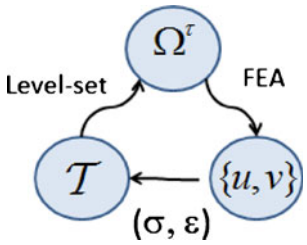

Fig. 5 Fixed point iteration involving three quantities

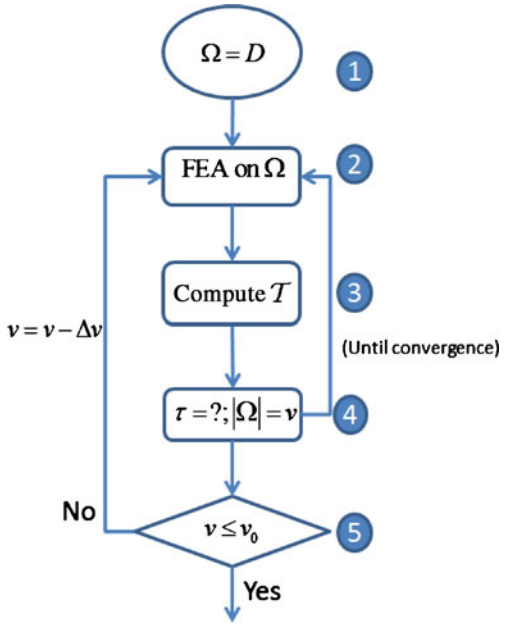

Fig. 6 An overview of the PareTO algorithm

In other words, in Step-5 of Fig. 6, an additional check $\sigma \leq \sigma_{\max}$ is imposed over all the elements, and the algorithm will generate a series of pareto-optimal topologies until the stress (in any element) exceeds a prescribed value. Such topologies will be referred to here as *stress-constrained compliance minimized (SCCM) topologies.* As expected, and illustrated later on, SCCM topologies are sub-optimal.

4.3 Stress constrained stress minimization

In contrast, one can define a stress topological sensitivity field T_S that will capture the sensitivity of the maximum stress (in a global sense) with respect to a topological change. Specifically a global stress measure is defined here via the popular p-norm (Le et al. 2010):

$$S = \left(\sum_e (\sigma_e)^p \right)^{1/p} \tag{4.4}$$

Now consider modifying the problem in (4.3) to a stress objective problem (with a finite compliance constraint to avoid zero-volume case):

$$\begin{aligned} &\underset{\Omega \subset D}{Min} \{S, |\Omega|\} \\ &\sigma \leq \sigma_{\max} \text{ in } \Omega \\ &J \leq J_{\max} \end{aligned} \tag{4.5}$$

In order to solve the above problem via the PareTO method, one must compute the topological sensitivity of the quantity S. Towards this end, recall that the sensitivity of S with respect to a nodal displacement $\hat{u}_n$ is given by:

$$\begin{aligned} g(n) = -\frac{\partial S}{\partial \hat{u}_n} = -\frac{1}{p} \left(\sum_e (\sigma_e)^p \right)^{1/p-1} \\ \times \left[\sum_e p\,(\sigma_e)^{p-1} \frac{\partial \sigma_e}{\partial \hat{u}_n} \right] \end{aligned} \tag{4.6}$$

Recall that the von Mises stress σ_e (in 3-D) is given by:

$$\sigma_e = \frac{1}{\sqrt{2}} \sqrt{\begin{aligned} &(\sigma_{11}-\sigma_{22})^2 + (\sigma_{11}-\sigma_{33})^2 + (\sigma_{22}-\sigma_{33})^2 \\ &+ 6\,(\sigma_{12}\sigma_{12} + \sigma_{13}\sigma_{13} + \sigma_{23}\sigma_{23}) \end{aligned}} \tag{4.7}$$

where the individual stresses are related to the nodal displacements via:

$$\{\sigma\}_{(6,1)} = [D]_{(6,6)} [B]_{(6,24)} \{u\}_{(24,1)} \tag{4.8}$$

In the above equation $[D]$ is the usual material tensor, $[B]$ is the gradient matrix, and

$$\begin{aligned} \{\sigma\}_{(6,1)} &= \left\{ \sigma_{11} \quad \sigma_{22} \quad \sigma_{33} \quad \sigma_{12} \quad \sigma_{13} \quad \sigma_{23} \right\}^T \\ \{\hat{u}\}_{(24,1)} &= \left\{ u_1 \quad v_1 \quad w_1 \quad \cdots \quad v_8 \quad w_8 \right\}^T \end{aligned} \tag{4.9}$$

Thus, one can easily show that:

$$g = -\frac{1}{p} \left(\sum_e (\sigma_e)^p \right)^{1/p-1} \left[\sum_e g_e \right] \tag{4.10}$$

where:

$$g_e = p(\sigma_e)^{p-2} \frac{1}{\sqrt{2}} \begin{pmatrix} (\sigma_{11} - \sigma_{22}) \left(F_{1,:} - F_{2,:} \right) + \\ (\sigma_{11} - \sigma_{33}) \left(F_{1,:} - F_{3,:} \right) + \\ (\sigma_{22} - \sigma_{33}) \left(F_{2,:} - F_{3,:} \right) + \\ 6\sigma_{12} F_{4,:} + 6\sigma_{13} F_{5,:} + 6\sigma_{23} F_{6,:} \end{pmatrix}$$

$$[F]_{(6,24)} = [D]_{(6,6)} [B]_{(6,24)} \tag{4.11}$$

Now g defines the 'right-hand-side' of an adjoint problem (Choi and Kim 2005):

$$K\lambda = -\nabla_u S \equiv g \tag{4.12}$$

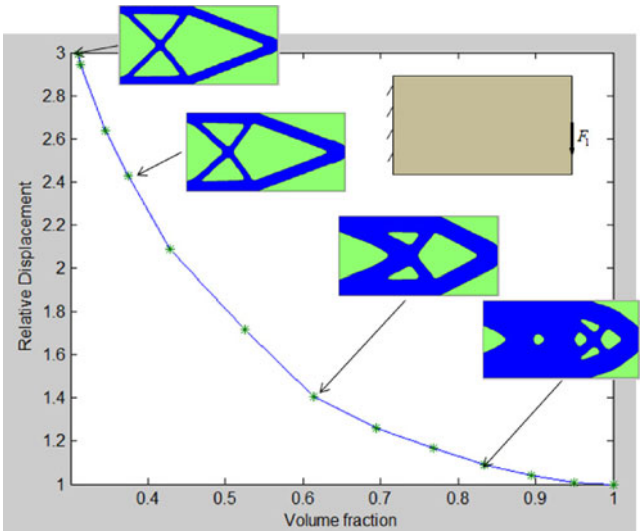

Fig. 7 Pareto-optimal topologies

The stiffness matrix is identical to that of (4.15). Once the adjoint field λ is computed the stress topological sensitivity field is defined (in 3-D) as Turevsky and Suresh (2011) and Feijoo et al. (2005):

$$\mathcal{T}_S = \frac{4}{1+\nu}\sigma(u) : \varepsilon(\lambda) - \frac{1-3\nu}{1-\nu^2} tr[\sigma(u)]\, tr[\varepsilon(\lambda)] \quad (4.13)$$

where $\sigma(u)$ refers to the stress tensor computed from the primary field, and $\varepsilon(\lambda)$ is the strain tensor computed from the adjoint field. Unlike the compliance topological sensitivity field, the stress topological sensitivity field T_S depends on the p-norm value. For $p = 4$, Fig. 8 illustrates the stress sensitivity field T_S. Observe that it closely resembles the compliance field T_J of Fig. 4.

On the other hand, Fig. 9 illustrates the T_S field for $p = 8$; the T_S field flattens out as p is increased.

4.4 Stabilization

One can now use the stress topological sensitivity field T_S (instead of the compliance field) directly in the PareTO algorithm of Fig. 6. There is however a numerical issue that one must address. Specifically, for the stress measure S in (4.4), a large value of p, say $p \geq 6$, is desirable to accurately capture the maximum stress. However, as one can observe in Fig. 9, for large values of p, the stress sensitivity field T_S typically flattens out far away from regions of high sensitivity. This poses a numerical challenge during level-set extraction. To overcome this challenge, we define a weighted topological sensitivity field per:

$$\mathcal{T} = w\mathcal{T}_S + (1-w)\mathcal{T}_J;\ 0 \leq w \leq 1 \quad (4.14)$$

where the weight w is determined dynamically as described in the next section (a similar concept of weighting stress and compliance objectives was exploited, for example, in the SIMP-based implementation of Yang and Chen 1996). An additional advantage of this method is that, when the stress topological sensitivity cannot distinguish between regions

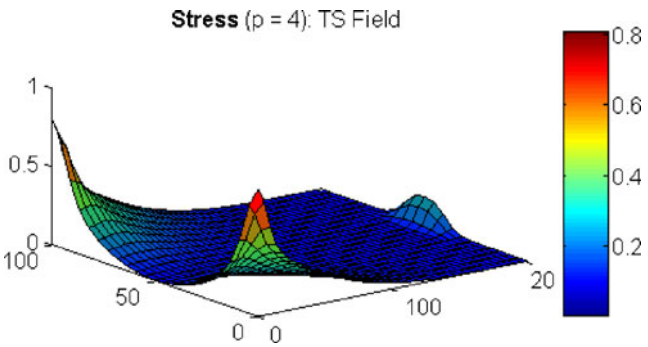

Fig. 8 A scaled stress topological sensitivity for $p = 4$

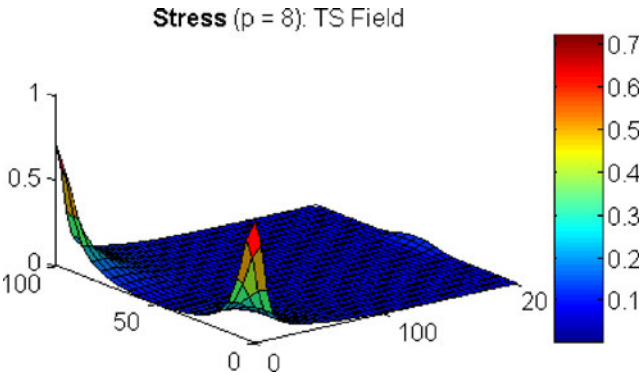

Fig. 9 Stress topological sensitivity for $p = 8$

of similar sensitivity (flat regions), the compliance sensitivity field induces a preference for a stiffer design, and thereby ensuring a finite compliance.

4.5 Stress constrained stress minimization

The modified PareTO algorithm, specifically for stress-constrained problems, is illustrated in Fig. 10. The details are as follows:

1. We start with $\Omega = D$, i.e., we start with a volume fraction of 1.0. The cutting-plane parameter τ is initialized to zero. The weighting factor w in (4.14) is set to a high-value (say 1).
2. A finite element analysis is carried out on Ω (also see next section).

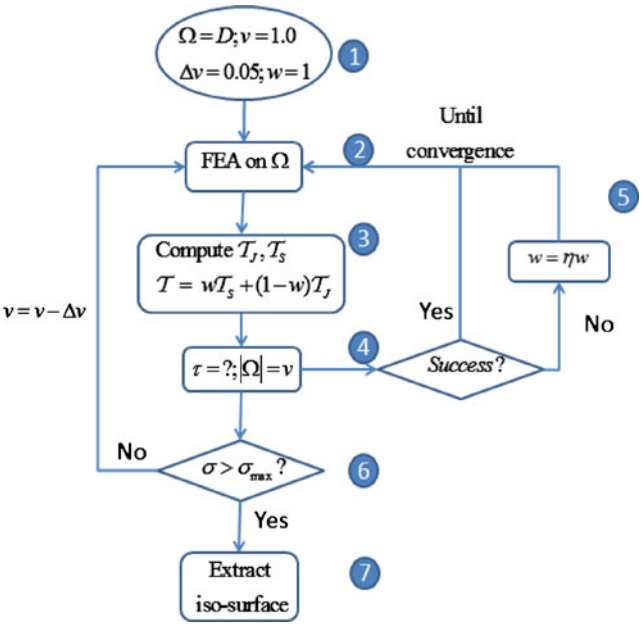

Fig. 10 The proposed algorithm

3. The compliance field T_J is computed via (3.2), the stress field T_S is computed via (4.13). Finally, the weighted field T is computed via (4.14), using the current weight w.
4. Given the weighted field T and the target volume fraction $v - \Delta v$, we seek the parameter τ such that $|\Omega^\tau|$ is equal to the target volume fraction. This is a binary-search algorithm between the maximum and minimum values of T.
5. As described earlier, the above level-set extraction may fail due to numerical difficulties, especially if the weight factor w is large. If the extraction fails, then w is reduced by a small factor; say $\eta = 0.9$. Steps 2 through 5 are repeated until convergence is reached.
6. Once the desired value of τ has been computed, if the stress constraint is satisfied, the volume is decremented and the algorithm returns to Step 2.
7. Once the algorithm terminates, one can extract the iso-surface extraction via classic marching-cubes algorithm (Lorensen and Cline 1987).

The resulting topology will be referred to *'stress constrained stress minimized (SCSM)'* topologies. Note that the stress-constraint is applies directly on the maximum von Mises stress (Fig. 10), and not on the p-norm measure. The latter is used primarily to compute the topological sensitivity and drive the topology.

Also note that elements are either 'in' or 'out', depending on the level-set, i.e., depending on (4.1). Partial elements lead to high-condition numbers, and are therefore avoided in the current work.

4.6 Finite element analysis

In the finite element analysis (Step 2 of Fig. 10), the design space is discretized into bi-linear quad elements in 2-D, and tri-linear hexahedral elements in 3-D; these elements offer a good compromise between accuracy and speed. The corresponding shape-functions and element-stiffness matrices can be found, for example, in Zienkiewicz and Taylor (2005).

In 2-D, the element stiffness matrices are assembled to form the global K matrix, and the following linear problem is solved using Matlab:

$$Ku = f \tag{4.15}$$

In 3-D, solution of such linear systems can be time and memory consuming. Therefore, instead of assembling the global stiffness matrix K we have chosen an 'assembly-free' (a.k.a. 'matrix-free') approach (Augarde et al. 2006). The linear system is solved implicitly using the assembly-free Jacobi-preconditioned conjugate-gradient (Jacobi-PCG) method (Saad 2003). Since PCG only requires a sparse matrix-vector multiplication (SpMV) Ku, this is implemented as follows:

$$Ku = \left(\sum_e K_e\right) u = \sum_e K_e u_e \tag{4.16}$$

In other words, the element solution vectors are multiplied by the (non-zero) element stiffness matrices, and then assembled. An additional benefit of a matrix-free implementation is that only the non-zero elements need to be considered. As the topology evolves, the computational cost reduces dramatically. Further, in the proposed method, the stiffness matrix is well-conditioned, and consequently, even the simple Jacobi-PCG converges rapidly.

For topology optimization, a fast linear solver is critical. In today's computational architecture, the primary computational cost in an iterative linear solver is memory-access (Arbenz et al. 2005). The cost of accessing elements of $_K$ can be dramatically reduced through assembly-free methods,details may be found in Suresh (2013) and Suresh and Yadav (2012).

5 Numerical examples

In this section, we present results from numerical experiments and compare the stress constrained compliance minimization (SCCM) topologies, and stress constrained stress minimization (SCSM) topologies.

The default parameters are as follows:

- The material properties are $E = 1$ and $v = 0.3$.
- In Steps 2 to 5 of the algorithm, the fixed-point iteration is assumed to have converged if the change in compliance is less than 5 %. The volume step-size set to 0.05.
- Unless otherwise noted, the p-norm value in all experiments is 8.

All experiments were conducted on a Windows 7 64-bit machine with the following hardware:

- Intel I7 960 CPU quad-core running at 3.2 GHz with 6 GB of memory; parallelization of CPU code was implemented through OpenMP commands.
- The graphics programmable unit (GPU) is an NVidia GeForce GTX 480 (480 cores) with 1.5 GB.

5.1 Tip-load cantilever

The first experiment involves the classic 2-D cantilever beam illustrated in Fig. 11, where one end of the beam is fixed, while a load is applied at the other end, as illustrated. The relative stress constraint was set to 1.2, as noted in the

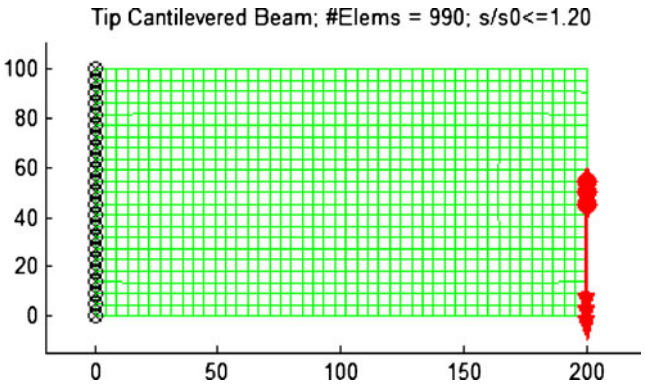

Fig. 11 The cantilevered beam problem

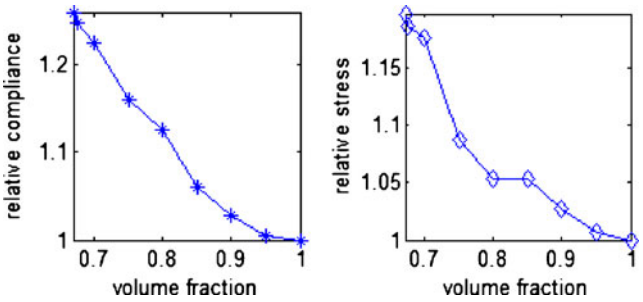

Fig. 13 History plots of relative compliance and relative maximum von Mises stress for the SCCM topology

title of Fig. 11. In other words, the maximum von Mises stress should not exceed 1.2 times the initial maximum von Mises stress. The domain was discretized into 990 quad elements as indicated.

The SCCM (stress constrained compliance minimized) topology, obtained by solving (4.3), is illustrated in Fig. 12. The algorithm terminated after 63 finite element operations, at a volume fraction of 0.67.

In all the numerical experiments that follow, the (relative) von Mises stress is displayed using a color-plot. Thus, in Fig. 12, the stress concentration occurs at the walls. Further note that the stress at the point of force application is relatively low since we have distributed the force over multiple-elements as illustrated in Fig. 11.

Figure 13 illustrates the compliance history and stress history of the algorithm, as a function of the volume fraction. As one can observe, the compliance of the final structure is approximately 25 % more than the initial compliance, while the maximum von Mises stress is 20 % more than the initial von Mises stress (as imposed by the constraint).

For the same structural problem, the SCSM (stress constrained stress minimized) topology, obtained by solving (4.5) with $p = 8$, is illustrated in Fig. 14. The algorithm terminated, after 190 finite element operations, at a volume fraction of 0.5. Thus, the SCSM topology is of a lower volume fraction compared to the SCCM topology.

Figure 15 illustrates the compliance history and stress history as a function of the volume fraction. The compliance of the final structure is approximately 80 % more than the initial compliance, while the maximum von Mises stress is 20 % more than the initial von Mises stress (satisfying the constraint). As expected, the SCSM topology is of a higher compliance.

Further note that the number of finite element operations for computing the SCSM is significantly larger. This is to be expected for two reasons: (1) in SCCM, for each iteration, only one finite element operation is required, whereas in SCSM, each iteration requires two finite element operations: one for the primary, and one for the adjoint, (2) since a lower volume fraction is reached in SCSM, larger number of iteration is to be expected.

In the proposed method, the Young's modulus of the material outside the evolving topology is set to zero. Consequently, the stiffness matrix is well-conditioned, and one can rely on iterative methods for solving the linear system of equations. This is particularly important in 3-D, where direct methods can be memory-intensive and slow. The number of conjugate-gradient iterations required as the topology evolves is illustrated in Fig. 16. In contrast, in the SIMP formulation, the number of conjugate gradient iterations can grow by a factor of 10 or more; see Suresh (2013).

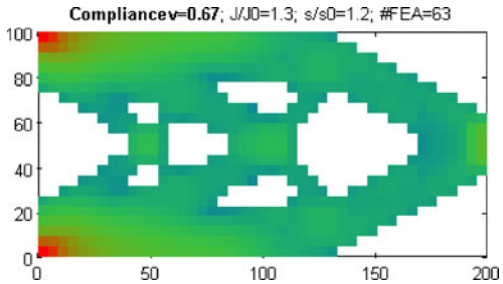

Fig. 12 Stress-constrained compliance minimized (SCCM) topology

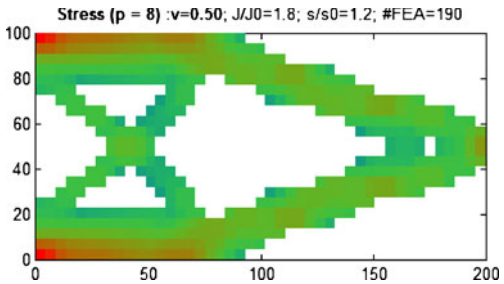

Fig. 14 Stress-constrained stress minimized (SCSM) topology

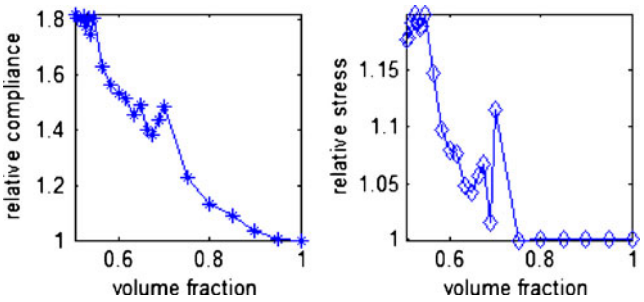

Fig. 15 History plots of relative compliance and relative maximum von Mises stress for the SCSM topology

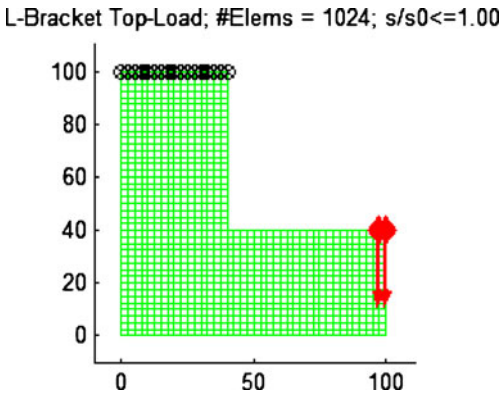

Fig. 17 An L-Bracket with top load

5.2 L-Bracket

The next experiment is the classic L-Bracket with top load, illustrated in Fig. 17. The relative stress constraint was set to 1.0, i.e., the maximum von Mises stress should not exceed the initial maximum von Mises stress.

The resulting SCCM (stress constrained compliance minimized) topology, obtained by solving (4.3), is illustrated in Fig. 18. The algorithm terminated after 66 finite element operations, at a volume fraction of 0.66. The final compliance is 20 % more than the initial compliance, while the stress meets the imposed constraint.

The SCSM topology is illustrated in Fig. 19; observe the significant difference in topology compared to Fig. 18. The algorithm terminated after 212 finite element operations, at a volume fraction of 0.47. The final compliance is 80 % more than the initial compliance, while the stress precisely the imposed constraint.

The above SCSM topology was generated with the p-norm value of 8. Figure 20 illustrates the SCSM topologies for various other values of the p-norm. Figure 20 also summarizes the final volume fractions, and the number of finite element operations at termination. Observe that for small values of the p-norm, the topology resembles the compliance topology. Thus $p \geq 6$ is usually desirable. On the other hand, the number of FEA increases as the p-norm increases, with no appreciable reduction in volume fraction. For this reason, we have chosen the value of $p = 8$ for the remainder of the experiments.

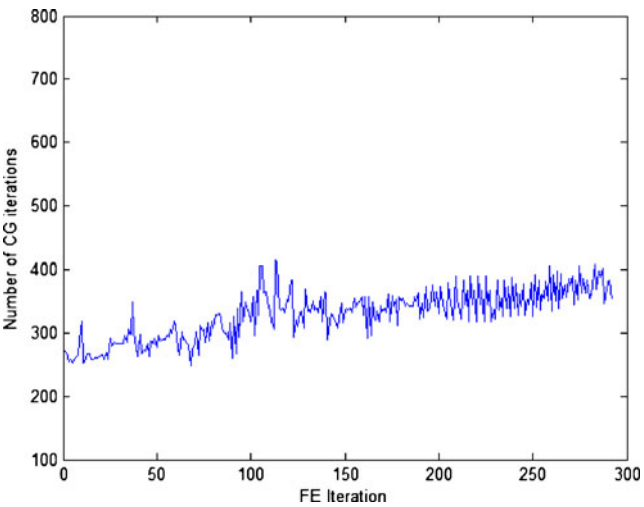

Fig. 16 Number of conjugate-gradient iterations during each of the finite element operations

5.3 L-Bracket: mesh refinement

We will now explore the sensitivity of the algorithms to mesh-refinement. Specifically in Fig. 21, 1980 quad-elements are used to discretize the geometry, as opposed to 1024 elements in the previous experiment.

The resulting SCCM (stress constrained compliance minimized) topology is illustrated in Fig. 22; the results are comparable to that of Fig. 18.

On the other hand, the SCSM topology illustrated in Fig. 23 is of a slightly lower volume fraction compared to that of Fig. 19, but similar topology.

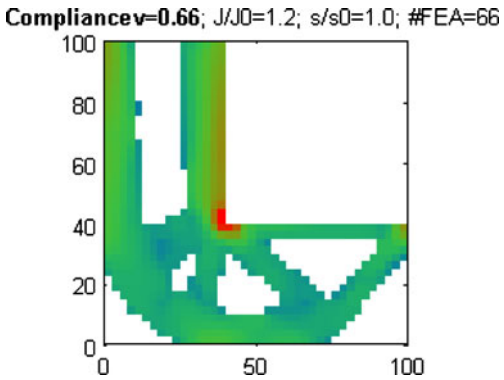

Fig. 18 SCCM topology

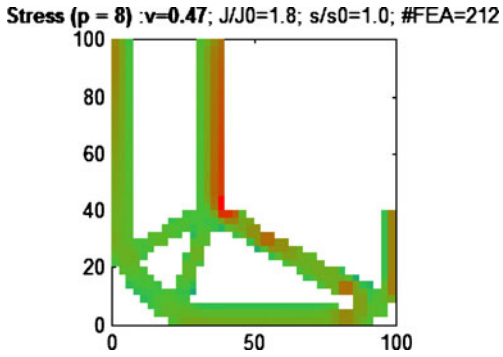

Fig. 19 SCSM topology

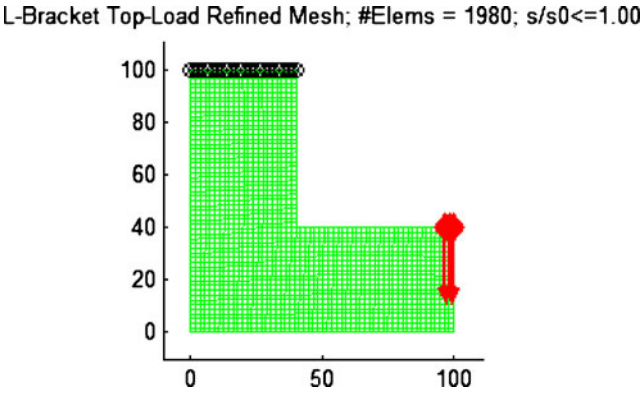

Fig. 21 A top-loaded L-Bracket with refined mesh

5.4 Michelle beam

The next experiment is the classic Michelle problem illustrated in Fig. 24. The relative stress constraint was set to 1.25.

The SCCM topology is illustrated in Fig. 25. The algorithm terminated after 71 finite element operations, at a volume fraction of 0.53. The final compliance is 50 % more than the initial compliance, while the stress meets the imposed constraint.

The SCSM topology is illustrated in Fig. 26; the topology is similar to the SCCM topology. However, the shape is significantly different. The algorithm terminated after 206 finite element operations, at a volume fraction of 0.39. The final compliance is 120 % more than the initial compliance, while the stress meets the imposed constraint.

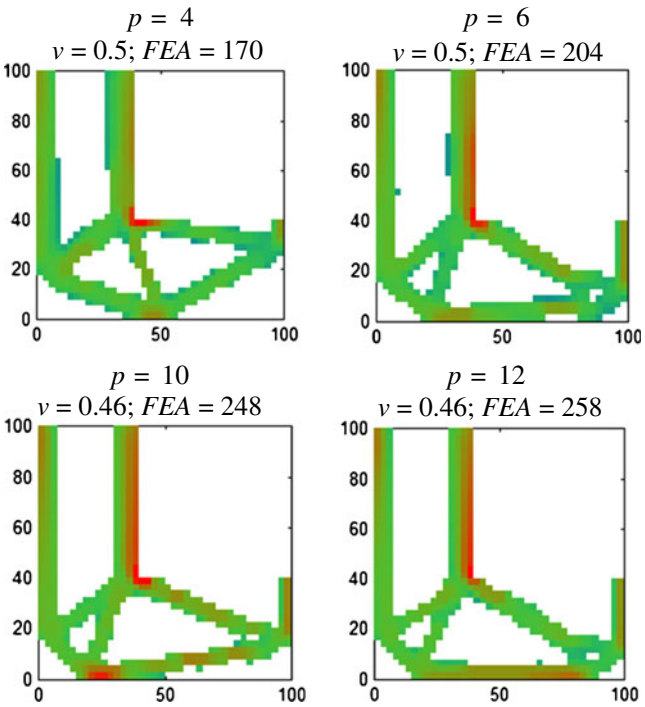

Fig. 20 SCSM topologies for various p-norm values

5.5 Mast

Next consider the mast problem (Amstutz and Novotny 2010) illustrated in Fig. 27. The relative stress constraint was set to 1.2.

The SCCM topology is illustrated in Fig. 28. The algorithm terminated after 72 finite element operations, at a volume fraction of 0.47. The final compliance is 110 % more than the initial compliance, while the stress meets the imposed constraint.

The SCSM topology is illustrated in Fig. 29. The algorithm terminated after 380 finite element operations, at a volume fraction of 0.39. The final compliance is 190 % more than the initial compliance, while the stress meets the imposed constraint.

5.6 Portal-frame (2-D)

The portal-frame problem discussed in Zhang et al. (2012) is illustrated in Fig. 30. Observe the stress-raisers at the three reentrant corners,please see Zhang et al. (2012) for further

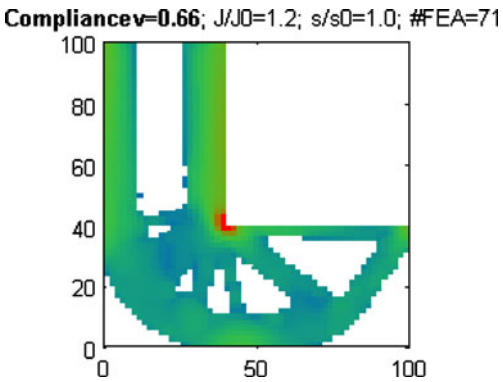

Fig. 22 SCCM topology

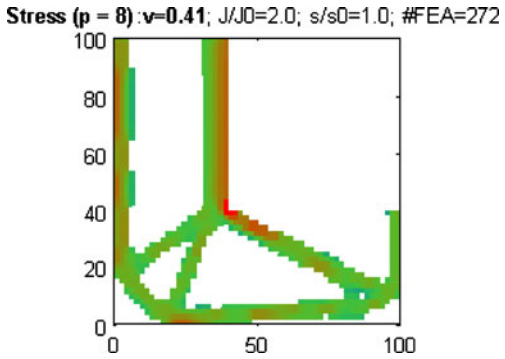

Fig. 23 SCSM topology

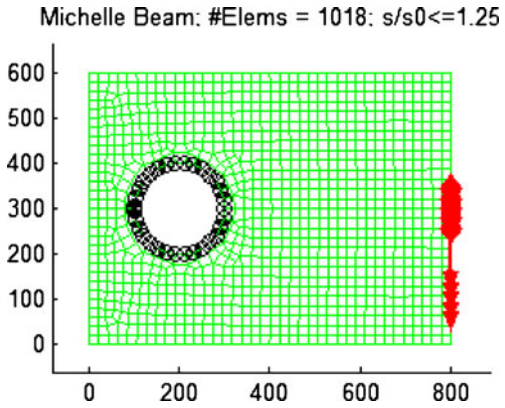

Fig. 24 Michelle-beam problem

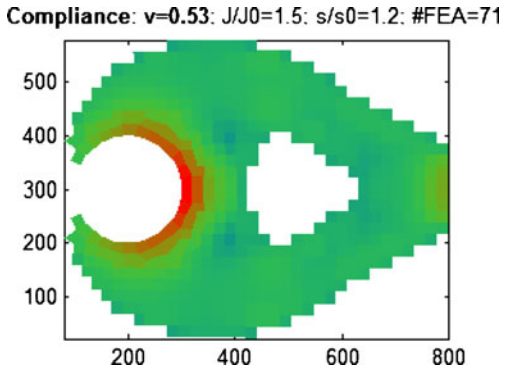

Fig. 25 SCCM topology

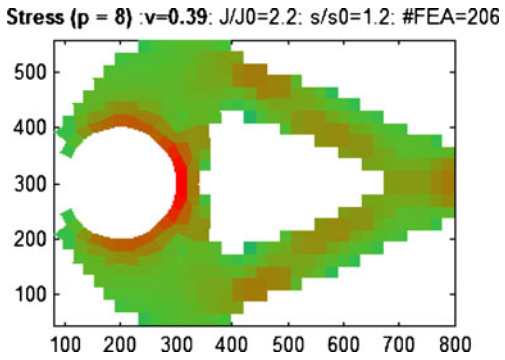

Fig. 26 SCSM topology

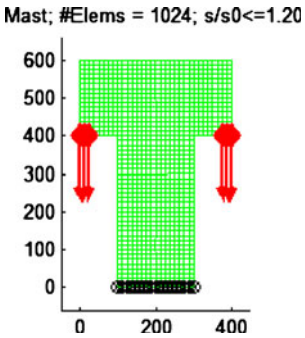

Fig. 27 Mast problem

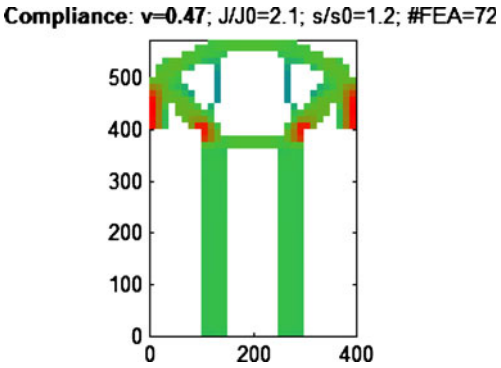

Fig. 28 SCCM topology for the mast problem

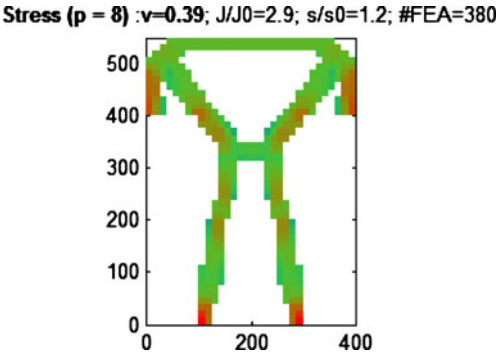

Fig. 29 SCSM topology for the mast problem

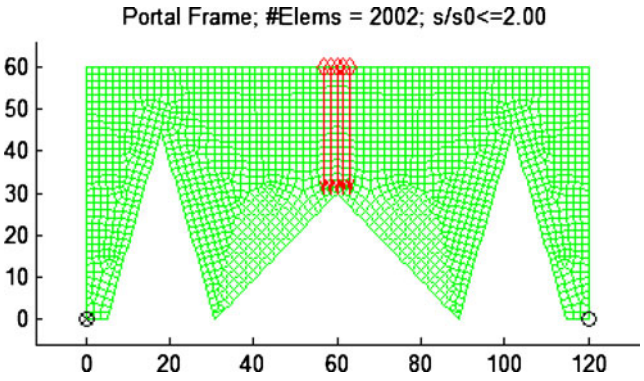

Fig. 30 The portal-frame problem (Zhang et al. 2012)

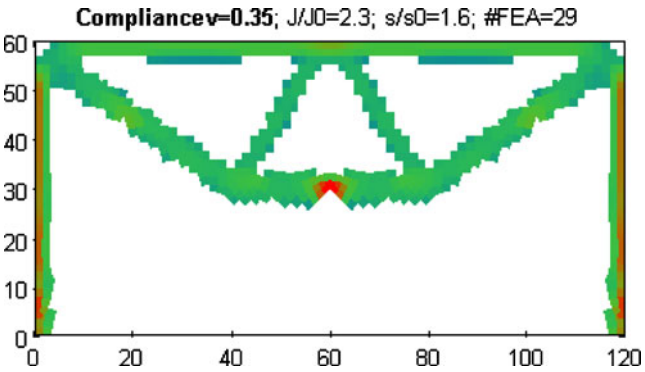

Fig. 31 SCCM topology for the portal-frame

details. The desired volume fraction was set to 0.35, and the relative max stress constraint was set to 2.0

The SCCM topology is illustrated in Fig. 31. The algorithm terminated after 29 finite element operations. Observe the stress concentration at the center

The SCSM topology is illustrated in Fig. 32. The fundamental difference is that the stress-raiser has been smoothen-out as illustrated. Consequently, the maximum stress is significantly lower.

5.7 L-Bracket (3-D)

Next, we repeat the L-Bracket example, but in 3-D, as illustrated in Fig. 33; the thickness of the L-bracket was 5 units. The problem is similar to that of Fig. 17, with identical stress constraint of 1.0. The 3-D geometry was voxelized (Suresh 2013) with approximately 11000 hexahedral elements, and the resulting finite element mesh has close to 50,000° of freedom. The problem was solved where the 3-D topological sensitivity field serves as the level-set.

The SCCM topology is illustrated in Fig. 34. The algorithm terminated after 49 finite element operations, at a volume fraction of 0.73 due to the stress constraint. The compliance of the final structure is approximately 11 % more than the initial compliance. The total time taken to find the optimal topology using the CPU was 95 s, and using the GPU was 35 s (Fig. 34).

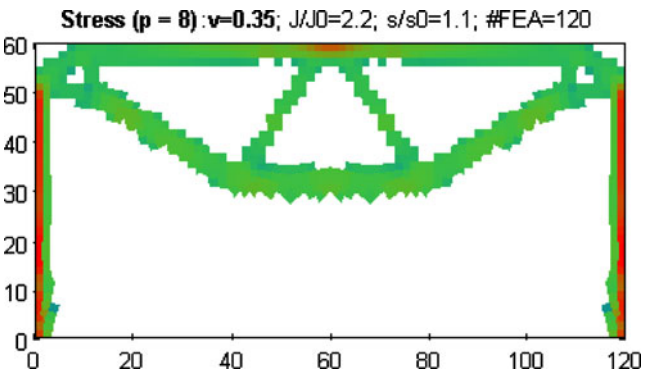

Fig. 32 SCSM topology for the portal frame

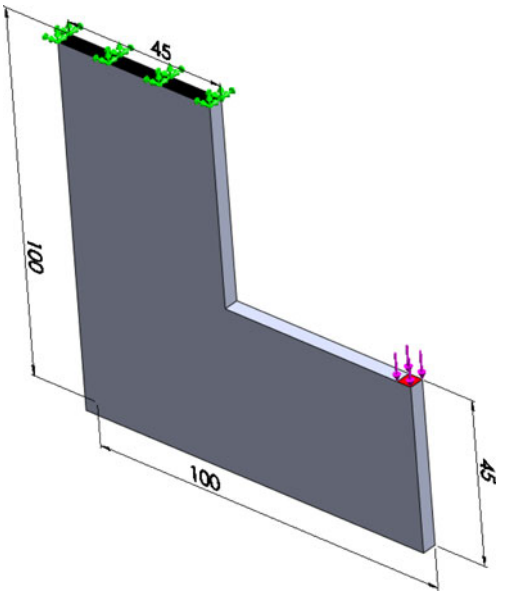

Fig. 33 The 3-D L-Bracket problem

For the same structural problem, the SCSM topology is illustrated in Fig. 35. The algorithm terminated after 284 finite element operations at a volume fraction of 0.357. The time taken on the CPU was approximately 10 min, and using the GPU was 213 s.

5.8 Knuckle design (3-D)

Finally, we consider the 'knuckle' geometry illustrated in Fig. 36, where the two horizontal holes were fixed, while a vertical force was applied on the vertical (inner) cylindrical face at the top. The 3-D geometry was voxelized with

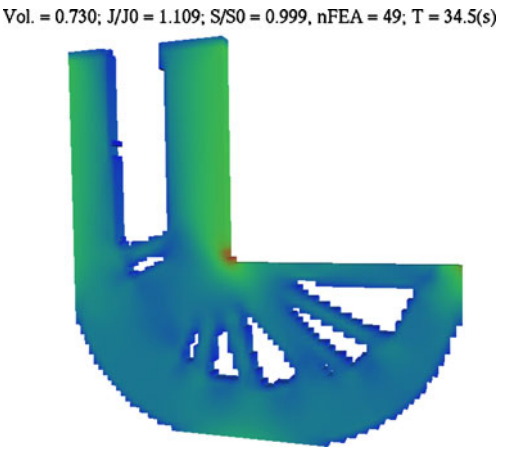

Fig. 34 SCCM topology for 3-D L-Bracket

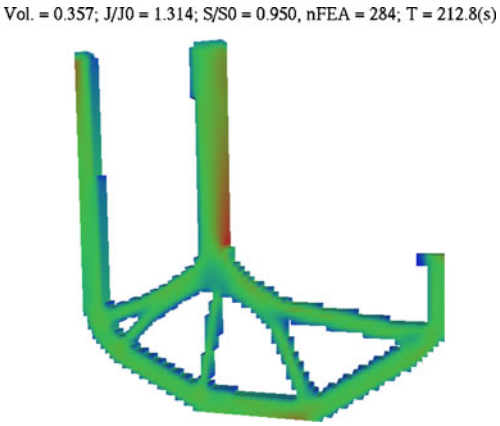

Fig. 35 SCSM topology for 3-D L-Bracket

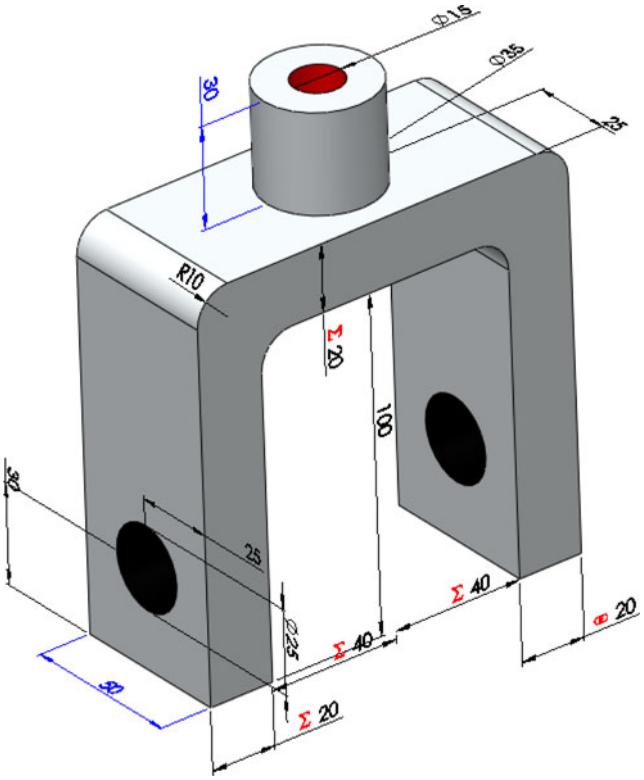

Fig. 36 Two views of the knuckle problem

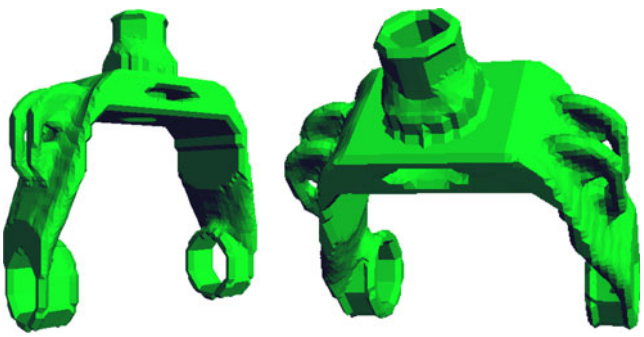

Fig. 37 Two views of the SCCM topology (volume fraction of 0.52)

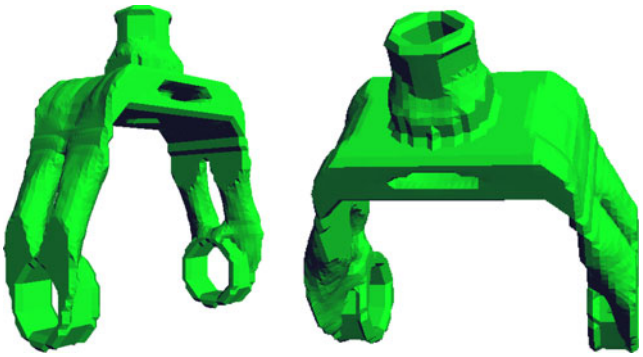

Fig. 38 Two views of the SCSM topology (volume fraction of 0.48)

approximately 27000 hexahedral elements, and the resulting finite element mesh had approximately 100,000° of freedom. The relative stress constraint was set to 1.2.

Two views of the SCCM topology are illustrated in Fig. 12. The algorithm terminated after 74 finite element operations, at a volume fraction of 0.52. The compliance of the final structure was approximately 25 % more than the initial compliance. The total time taken to find the optimal topology using the CPU was 140 s, and using the GPU, was 46 s (Fig. 37).

The SCSM topology is illustrated in Fig. 35; observe the significant difference in topology. The compliance of the final structure was approximately 43 % more than the initial compliance. The algorithm terminated after 286 finite element operations with a volume fraction of 0.48. The total time taken to find the optimal topology using the CPU was 140 s, and using the GPU, was 46 s (Fig. 38).

6 Conclusions

The main contribution of the paper is a new method for stress constrained topology optimization. As illustrated via numerical examples, the proposed is efficient and robust with respect to parameter changes. Further, the stress constraint is precisely satisfied at termination.

As reported by various authors, the topologies obtained via stress minimization are significantly different, and typically of a lower volume fraction, compared to topologies obtained via compliance minimization. Future work will focus on including other constraints including buckling and eigen-modes.

ParETO can be downloaded from www.ersl.wisc.edu.

References

Allaire G, Jouve F (2005) A level-set method for vibration and multiple loads structural optimization. Struct Des Optim 194(30–33):3269–3290

Allaire G, Jouve F (2008) Minimum stress optimal design with the level set method. Eng Anal Bound Elem 32(11):909–918

Allaire G, Jouve F, Toader AM (2002) A level-set method for shape optimization. Comput Rendus Math 334(12):1125–1130

Allaire G, Jouve F, Toader AM (2004) Structural optimization using sensitivity analysis and a level-set method. J Comput Phys 194(1):363–393

Amstutz S, Novotny AA (2010) Topological optimization of structures subject to Von Mises stress constraints. Struct Multidisc Optim 41(3):407–420

Arbenz P, Hetmaniuk UL, Lehoucq RB, Tuminaro RS (2005) A comparison of eigensolvers for large-scale 3D modal analysis using AMG-preconditioned iterative methods. Int J Numer Methods Eng 64(2):204–236

Augarde CE, Ramage A, Staudacher J (2006) An element-based displacement preconditioner for linear elasticity problems. Comput Struct 84(31–32):2306–2315

Bendsoe MP, Sigmund O (2003) Topology optimization: theory, methods and application, 2nd edn. Springer

Bruggi M, Duysinx P (2012) Topology optimization for minimum weight with compliance and stress constraints. Struct Multidisc Optim 46:369–384

Bruggi M, Venini P (2008) A mixed FEM approach to stress constrained topology optimization. Int J Numer Methods Eng 73(12):1693–1714

Céa J, Garreau S, Guillaume P, Masmoudi M (2000) The shape and topological optimization connection. Comput Methods Appl Mech Eng 188(4):713–726

Choi KK, Kim NH (2005) Structural sensitivity analysis and optimization I: linear systems. Springer, New York

Duysinx P, Bendsoe MP (1998) Topology optimization of continuum structures with local stress constraints. Int J Numer Methods Eng 43(8):1453–1478

Duysinx P, Miegroet LV, Lemaire E, Brüls O, Bruyneel M (2008) Topology and generalized shape optimization: why stress constraints are so important? Int J Simul Multidisc Des Optim 2:253–258

Eschenauer HA, Olhoff N (2001) Topology optimization of continuum structures: a review. Appl Mech Rev 54(4Esch01):331–389

Eschenauer HA, Kobelev VV, Schumacher A (1994) Bubble method for topology and shape optimization of structures. Struct Optim 8:42–51

Feijoo RA, Novotny AA, Taroco E, Padra C (2005) The topological-shape sensitivity method in two-dimensional linear elasticity topology design. In: Applications of computational mechanics in structures and fluids. CIMNE

Gopalakrishnan SH, Suresh K (2008) Feature sensitivity: a generalization of topological sensitivity (This work was partly or wholly funded by the National Science Foundation). Finite Elem Anal Des 44(11):696–704

Guo X, Cheng GD (2004) Epsilon-continuation approach for truss topology optimization. Acta Mech Sin 20(5):526–533

Guo X, Zhang WS, Wang YU, Wei P (2011) Stress-related topology optimization via level set approach. Comput Methods Appl Mech Eng 200:3439–3452

He L, Kao C-Y, Osher S (2007) Incorporating topological derivatives into shape derivatives based level set methods. J Comput Phys 225(1):891–909

James KA, Lee E, Martins JRRA (2012) Stress-based topology optimization using an isoparametric level set method. Finite Elem Anal Des 58:20–30

Kocvara M, Stingl M (2012) Solving stress constrained problems in topology and material optimization. Struct Multidisc Optim 46(1):1–15

Le C (2010) Developments in topology and shape optimization. PhD thesis, University of Illinois at Urbana-Champaign, Urbana-Champaign

Le C, Norato JA, Bruns TE, Ha C, Tortorelli DA (2010) Stress-based topology optimization for continua. Struct Multidisc Optim 41(4):605–620

Lorensen WE, Cline HE (1987) Marching cubes: a high resolution 3D surface reconstruction algorithm. Comput Graph (Proc. of SIGGRAPH) 21(4):163–169

Norato JA, Bendsøe MP, Haber RB, Tortorelli DA (2007) A topological derivative method for topology optimization. Struct Multidisc Optim 33:375–386

Novotny AA (2006) Topological-shape sensitivity method: theory and applications. Solid Mech Appl 137:469–478

Novotny AA, Feijóo RA, Padra C, Taroco E (2005) Topological derivative for linear elastic plate bending problems. Control Cybern 34(1):339–361

Novotny AA, Feijoo RA, Taroco E (2007) Topological sensitivity analysis for three-dimensional linear elasticity problem. Comput Methods Appl Mech Eng 196(41–44):4354–4364

Paris J, Navarrina F, Colominas I, Casteleiro M (2009) Topology optimization of continuum structures with local and global stress constraints. Struct Multidisc Optim 39(4):419–437

Qiu GY, Li XS (2010) A note on the derivation of global stress constraints. Struct Multidisc Optim 40(1–6):625–628

Rozvany GIN (2009) A critical review of established methods of structural topology optimization. Struct Multidisc Optim 37(3):217–237

Saad Y (2003) Iterative methods for sparse linear systems. SIAM, Philadelphia, PA

Sigmund O (2001) A 99 line topology optimization code written in Matlab. Struct Multidisc Optim 21(2):120–127

Sokolowski J, Zochowski A (1999) On topological derivative in shape optimization. SIAM J Control Optim 37(4):1251–1272

Stump FV, Silva ECN, Paulino G (2007) Optimization of material distribution in functionally graded structures with stress constraints. Commun Numer Methods Eng 23(6):535–551

Suresh K (2010) A 199-line Matlab code for Pareto-optimal tracing in topology optimization. Struct Multidisc Optim 42(5):665–679

Suresh K (2013) Efficient generation of large-scale Pareto-optimal topologies (This work was partly or wholly funded by the National Science Foundation). Struct Multidisc Optim 47(1): 49–61. doi:10.1007/s00158-012-0807-3

Suresh K, Yadav P (2012) Large-scale modal analysis on multi-core architectures. In: Proceedings of the ASME 2012 international design engineering technical conferences & computers and information in engineering conference, Chicago, IL

Svanberg K, Werme M (2007) Sequential integer programming methods for stress constrained topology optimization. Struct Multidisc Optim 34(4):277–299

Turevsky I, Suresh K (2007) Generalization of topological sensitivity and its application to defeaturing (This work was partly or wholly funded by the National Science Foundation). In: ASME IDETC conference, Las Vegas

Turevsky I, Suresh K (2011) Tracing the envelope of the objective-space in multi-objective topology optimization (This work was partly or wholly funded by the National Science Foundation) Presented at the ASME IDETC/CIE conference, Washington, DC

Turevsky I, Gopalakrishnan SH, Suresh K (2009) An efficient numerical method for computing the topological sensitivity of arbitrary shaped features in plate bending (This work was partly or wholly funded by the National Science Foundation). Int J Numer Methods Eng 79:1683–1702

Wang MY, Wang X, Guo D (2003) A level set method for structural topology optimization. Comput Methods Appl Mech Eng 192:227–246

Wang S, Sturler ED, Paulino G (2007) Large-scale topology optimization using preconditioned Krylov subspace methods with recycling. Int J Numer Methods Eng 69(12):2441–2468

Xia Q, Shi T, Liu S, Wang MY (2012) A level set solution to the stress-based structural shape and topology optimization. Comput Struct 90–91:55–64

Yalamanchili VK, Kumar AV (2012) Topology optimization of structures using a global stress measure. In: Proceedings of the ASME 2012 international design engineering technical conferences & computers and information in engineering conference. Chicago, IL

Yang RJ, Chen CJ (1996) Stress-based topology optimization. Struct Optim 12:98–105

Zhang WS, Guo X, Wang MY, Wei P (2012) Optimal topology design of continuum structures with stress concentration alleviation via level set method. Int J Numer Methods Eng. doi:10.1002/10.1002/nme.4416

Zienkiewicz OC, Taylor RL (2005) The finite element method for solid and structural mechanics. Elsevier